IOP Conf. Series: Materials Science and Engineering **424** (2018) 012014 doi:10.1088/1757-899X/424/1/012014

# Convective end effects in annular linear induction pumps

Yves Delannoy[1], Elena Martin-Lopez[1,2], Fabrice BENOIT[2]

[1] Univ. Grenoble Alpes, CNRS, Grenoble INP, SIMaP, F-38000 Grenoble, France
[2] CEA Cadarache /DTN/STCP/LCIT, 13108 St Paul lès Durance, France

*Corresponding author : yves.delannoy@simap.grenoble-inp.fr*

**Abstract**
This paper presents a simplified theory giving the performance of an annular linear electromagnetic pump, such as the liquid sodium pumps foreseen in some GenIV nuclear reactors. End effects are taken into account with a new model enabling physical interpretation.

## Introduction

An annular linear induction pump (ALIP) is an electromagnetic device producing a traveling magnetic field in an annular section, where an electrically conductive fluid is flowing against an adverse pressure gradient (produced by a dissipative hydraulic circuit). Its linear inductor, placed around the annular sodium channel, produces a radial magnetic field $B_r$ across the sodium up to the central (passive) magnetic core. The three phase arrangement of coils produces roughly a progressive sine wave for $B_r$, traveling at velocity $U_B$ along the axis, over the inductor length $L$.
For such large size pumps (axial length ~ meters, axial velocity ~ meters per second), the magnetic field can be significantly modified by the axial velocity $U_z$ (high magnetic Reynolds number), especially in the end regions ($x=\pm L/2$). The performance curve of the pump is affected (stall phenomena at high slip velocity), with an unstable zone [1] where partial stall may occur. Such instabilities have been observed on a Japanese pump tested for similar applications [2].
The goal of this paper is to investigate the end effects with an analytical model simpler than [3], based on existing theories for linear motors [4]. The model results will be compared to performance curves calculated for the PEMDYN pump (Figure 1 a), installed at CEA to provide experimental results in the frame of the ASTRID project (a future fast-breeder GENIV sodium reactor). PEMDYN has a sodium flowrate up to 1500m$^3$/h, and a pressure up to 2.5bar.

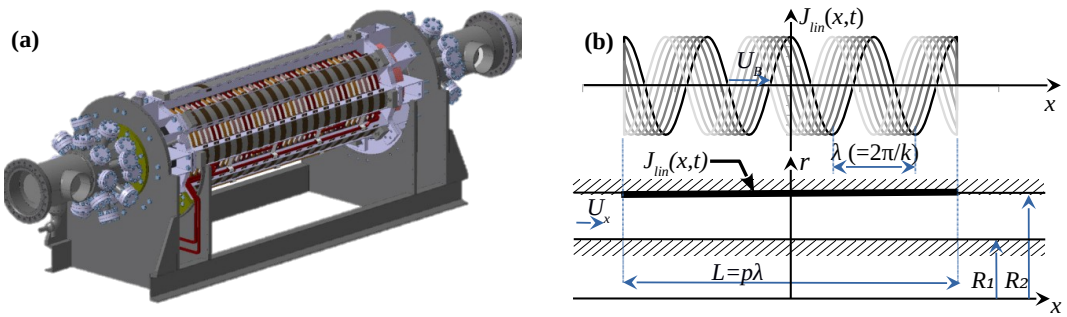


Figure 1: The PEMDYN [1] experimental pump (a), and its idealized model (b)

## Electromagnetic model

The geometry considered is rotationally symmetric and axially infinite (Figure 1 b), except the inductor, simplified to a thin sheet of current (heavy line at $r=R_2$) where the linear current density follows a progressive sine wave with wavelength $\lambda$. The length of the inductor is $L=p\lambda$, where $p$ is the "number of pole pairs", and the wavenumber is defined as $k=2\pi/\lambda$. The yokes (dashed zones in Figure 1 b) are supposed magnetically perfect ($\mu_r\sim\infty$) and in contact with the liquid sodium or current sheet at $r=R_1$ and $R_2$. The induction equation (1) is written using the azimuthal component $A_\theta$ of the magnetic vector potential, and the axial component $U_z$ of the velocity. Other components of both vector fields are zero because of the rotational symmetry and the developed flow conditions along $z$.

$$\frac{\partial^2 A_\theta}{\partial x^2}+\frac{\partial^2 A_\theta}{\partial r^2}+\frac{1}{r}\frac{\partial A_\theta}{\partial r}-\frac{A_\theta}{r^2}=\mu_0\sigma\left(\frac{\partial A_\theta}{\partial t}+U_x\frac{\partial A_\theta}{\partial x}\right) \quad \text{with} \quad B_x=\frac{\partial A_\theta}{\partial r}+\frac{A_\theta}{r} \quad \text{and} \quad B_r=-\frac{\partial A_\theta}{\partial x} \qquad (1)$$

The boundary conditions at the magnetic yokes impose $B_z=0$ at $r=R_1$ and $B_z=\mu_0\mathrm{Re}\{J_{lin}(x)e^{-i\omega t}\}$ at $r=R_2$ (where $J_{lin}(x)=J_{peak}e^{ikx}$ for $-p\lambda/2<x<p\lambda/2$, and $J_{lin}(x)=0$ elsewhere). Looking for an harmonic solution $A_\theta(x,r,t)=\mathrm{Re}\{A_\theta(x,r)e^{-i\omega t}\}$, equation (1) and its boundary conditions can be converted to a two dimensional boundary value problem for the

complex field $A_\theta(r,t)$, written below using the dimensionless variables $\alpha=A_\theta/(\mu_0 J_{peak}/k)$, $\eta=(r-R_1)/(R_2-R_1)$ and $\xi=kx$. Introducing the velocity $U_B=\omega/k$ of the travelling field, the dimensionless flowrate $q=U_x/U_B$ to represent the fluid velocity, which is supposed independent of $r$ in this paper, the problem can be written:

$$\begin{cases} \dfrac{\partial^2\bar{\alpha}}{\partial\eta^2}+\left(\dfrac{H_R}{1+H_R\eta}\right)\dfrac{\partial\bar{\alpha}}{\partial\eta}+\left(\dfrac{H_R}{1+H_R\eta}\right)^2\bar{\alpha}=H_\lambda^2\left[-\dfrac{\partial^2\bar{\alpha}}{\partial\xi^2}-R_{mB}\left(\mathrm{i}\,\bar{\alpha}-q\dfrac{\partial\bar{\alpha}}{\partial\xi}\right)\right] \\ \dfrac{\partial\bar{\alpha}}{\partial\eta}+\left(\dfrac{H_R}{1+H_R\eta}\right)\bar{\alpha}=\begin{cases}0 & \text{for } \eta=0\\ H_\lambda\bar{\varphi}_{lin} & \text{for } \eta=1\end{cases} \quad \text{with} \quad \bar{\varphi}_{lin}(\xi)=\begin{cases}e^{\mathrm{i}\xi} & \text{for } |\xi|<\pi p\\ 0 & \text{for } |\xi|>\pi p\end{cases} \end{cases} \tag{2}$$

where the geometrical parameters $H_R=(R_2-R_1)/R_1$, $H_\lambda=k(R_2-R_1)$ and $p$ measure respectively the influence of axisymmetric terms ($H_R\to 0$ when the domain is thin compared to its radius), the thickness of the magnetic gap compared to the reduced wavelength $\lambda/2\pi$, and the length of the inductor (in wavelengthes). The working point of the pump is represented by the magnetic Reynolds number $R_{mB}=\mu_0\sigma U_B/k$ (for a given pump and fluid, it depends on the generator pulsation $\omega$) and by $q$, the fluid flowrate divided by the flowrate at synchronism.

Following [3] and [4], the problem can be solved using Fourier transforms along $\xi$, i.e. superposing solutions of the form $\hat{\alpha}_\kappa e^{i\kappa\xi}$ where $\kappa$ is a continuously varying real wavelength and the complex amplitude of this mode. However, we will use here only three modes, one at $\kappa=1$ to represent the solution that we would have for an infinite pump, and two others with complex wavenumbers $\kappa_u$ and $\kappa_d$ representing the end effects generated by the inlet and outlet of the inductor and diffused upstream ($\mathrm{Im}(\kappa_u)<0$ so that this mode vanishes upstream) or convected downstream ($\mathrm{Im}(\kappa_d)>0$ so that this convected mode disapears downstream by joule dissipation). Those end effect modes are requested to verify (2) with zero source term $\bar{\varphi}_{lin}$, so they can be added to the infinite pump solution without destroying it far from the ends.

Therefore we look for solutions under the form $\bar{\alpha}=\hat{\alpha}_{iu}e^{i\kappa_u(\xi+\pi p)}$ for $\xi<-\pi p$ ; $\bar{\alpha}=\hat{\alpha}_{od}e^{i\kappa_d(\xi-\pi p)}$ for $\xi>\pi p$, and $\bar{\alpha}=\hat{\alpha}_{id}e^{i\kappa_d(\xi+\pi p)}+\hat{\alpha}_1 e^{i\xi}+\hat{\alpha}_{ou}e^{i\kappa_u(\xi-\pi p)}$ for $-\pi p<\xi<\pi p$ (subscripts $i$,$o$ for inlet, outlet). Requesting the induction problem (2) to be fulfilled in every subdomain, we get an ordinary differential problem with complex unknown $\hat{\alpha}_\kappa(\eta)$ for each mode of wavelength $\kappa$, and we will connect the domains requesting that $\bar{\alpha}$ and $\partial\bar{\alpha}/\partial\xi$ are continuous at $\xi=\pm\pi p$.

**Analytical solution**

For a mode with complex wavenumber $\kappa$ and amplitude $\hat{\alpha}_\kappa(\eta)$, (2) becomes:

$$\frac{d^2\hat{\alpha}_\kappa}{d\eta^2}+\left(\frac{H_R}{1+H_R\eta}\right)\frac{d\hat{\alpha}_\kappa}{d\eta}-\left(\frac{H_R}{1+H_R\eta}\right)^2\hat{\alpha}_\kappa=H_\lambda^2\left[\kappa^2-\mathrm{i}\,R_{mB}(1-\kappa q)\right]\hat{\alpha}_\kappa \tag{3}$$

with

$$\frac{d\hat{\alpha}_\kappa}{d\eta}+\left(\frac{H_R}{1+H_R\eta}\right)\hat{\alpha}_\kappa=\begin{cases}0 & \text{at } \eta=0\\ 0 & \text{at } \eta=1 \text{ for } \kappa=\kappa_u,\kappa_d\\ H_\lambda & \text{at } \eta=1 \text{ for } \kappa=1\end{cases} \tag{4}$$

For $\kappa=\kappa_u$ or $\kappa=\kappa_d$, having a non zero solution (singular value problem) requires that $\kappa^2-\mathrm{i}R_{mB}(1-\kappa q)=0$ (two solutions). Since $\kappa_u$ has negative imaginary part, and writing $\sqrt{(z)}$ for the complex square root with positive real part, we get:

$$\kappa_u=-i\frac{qR_{mB}}{2}\left(1+\sqrt{1-\mathrm{i}\frac{4}{q^2R_{mB}}}\right) \quad \text{and} \quad \kappa_d=-i\frac{qR_{mB}}{2}\left(1-\sqrt{1-\mathrm{i}\frac{4}{q^2R_{mB}}}\right) \tag{5}$$

For large values of $q^2R_{mB}$, the upstream mode is damped over a short axial distance $1/(qR_{mB})$ without oscillations (counterflow diffusion), whereas the downstream mode is a weakly damped traveling wave propagating at the fluid velocity $q$ (convection by the flow of current loops that cannot change rapidely). Such modes were yet presented in [6], but not used inside the inductor zone. A profile for the phasor of those modes can be obtained from (3),(4) without right hand side: it becomes uniform for quasi flat pumps, i.e. for a small channel height compared to its radius ($H_R\to 0$).

The infinite pump solution ($\kappa=1$) of (3) with boundary conditions (4) is written analytically from the modified Bessel functions of first kind ($I_0$, $I_1$) and second kind ($K_0$, $K_1$) divided by their exponential trend at infinity: $I_{0e}(z)=I_0(z)/\mathrm{e}^{\mathrm{Re}(z)}$, $I_{1e}(z)=I_1(z)/\mathrm{e}^{\mathrm{Re}(z)}$, $K_{0e}(z)=K_0(z)/\mathrm{e}^{-\mathrm{Re}(z)}$, and $K_{1e}(z)=K_1(z)/\mathrm{e}^{-\mathrm{Re}(z)}$, using the slip magnetic Reynolds number $R_{mS}=(1-q)R_{mB}$:

$$\hat{\alpha}_1=\frac{H_\lambda}{c_1}\frac{e^{\mathrm{Re}(c_1)\eta}K_{0e}(\rho_1)I_{1e}\left[\left(\frac{1}{H_R}+\eta\right)c_1\right]+e^{-\mathrm{Re}(c_1)\eta}I_{0e}(\rho_1)K_{1e}\left[\left(\frac{1}{H_R}+\eta\right)c_1\right]}{e^{\mathrm{Re}(c_1)}I_{0e}(\rho_2)K_{0e}(\rho_1)-e^{-\mathrm{Re}(c_1)}I_{0e}(\rho_1)K_{0e}(\rho_2)} \quad \text{with} \quad \begin{cases}\rho_1=\left(\dfrac{1}{H_R}\right)c_1 \;;\; \rho_2=\left(\dfrac{1}{H_R}+1\right)c_1\\ c_1=H_\lambda\sqrt{1-\mathrm{i}R_{mS}}\end{cases} \tag{6}$$

Under that form, the solution can be developed for $H_R\to 0$, (quasi-flat pumps) to retrieve the classical solution of (3),(4) for $H_R=0$. Furthermore, if $H_\lambda\ll 1$, the complex coefficient $c_1$ has a small module and this quasi-flat solution may be further developed to give the thin channel solution ($H_R\ll 1$, $H_\lambda\ll 1$ means that the channel height is small compared to $R_1\approx R_2$ and compared to $\lambda$):

$$\hat{\alpha}_1=\frac{H_\lambda}{c_1}\frac{\cosh(c_1\eta)}{\sinh(c_1)} \text{ for } H_R\ll 1 \text{ and } \hat{\alpha}_1=\frac{1}{H_\lambda(1-\mathrm{i}R_{mS})}+\frac{H_\lambda\eta^2}{2} \text{ for } H_R\ll 1, H_\lambda\ll 1 \quad (7)$$

Notice that for thin channels, the distribution of $\hat{\alpha}_1$ is approximately constant along $\eta$, but its variation with $\eta$ is useful to calculate $B_x$ and then verify the boundary conditions. The continuity of $\bar{\alpha}$ and $\partial\alpha/\partial\xi$ cannot be exactly satisfied in the general case for any value of $\eta$, because the three modes do not have the same profile along $\eta$. Writing $\bar{\alpha}(\xi,\eta)=\hat{\alpha}_1(\eta)\bar{f}(\xi)$ is thus an approximation, but it becomes precise for thin channels ($H_R\ll 1$ and $H_\lambda\ll 1$), where all profiles become uniform. We will use such a formula in all cases because real nuclear pumps have indeed $H_R\ll 1$ and their $H_\lambda$ is small enough to have reasonably uniform profiles of $\hat{\alpha}$. Writing the continuity conditions without influence of the outlet on inlet ($|\exp(2\mathrm{i}\pi K_u p)|\ll 1$), we get:

$$\bar{f}(\xi)=\begin{cases} a_{iu}e^{\mathrm{i}\kappa_u(\xi+\pi p)} & \text{for } \xi<-\pi p \\ a_{id}e^{\mathrm{i}\kappa_d(\xi+\pi p)}+e^{\mathrm{i}\xi}+a_{ou}e^{\mathrm{i}\kappa_u(\xi-\pi p)} & \text{for } -\pi p<\xi<\pi p \\ a_{od}e^{\mathrm{i}\kappa_d(\xi-\pi p)} & \text{for } \xi>\pi p \end{cases} , \quad \begin{cases} a_{iu}=(-1)^p\dfrac{1-\kappa_d}{\kappa_u-\kappa_d} \;;\; a_{ou}=-a_{id} \\ a_{id}=(-1)^p\dfrac{1-\kappa_u}{\kappa_u-\kappa_d} \;;\; a_{od}=-a_{id}\left(1-e^{2\mathrm{i}\pi p\kappa_d}\right) \end{cases} \quad (8)$$

From the radial distribution (6) or (7) combined to the axial distribution (8), it is now possible to calculate the current density $\bar{j}_\theta=\sigma(\mathrm{i}\omega\bar{A}_\theta-U_x\partial\bar{A}_\theta/\partial x)$ and the radial magnetic field density $\bar{B}_r=-\partial\bar{A}_\theta/\partial x$, to get the volumetric force density $\boldsymbol{F}=\boldsymbol{j}\times\boldsymbol{B}$. The axial component of $\boldsymbol{F}$ has a mean part $F_{x\,avg}=-\mathrm{Re}(\bar{j}_\theta\bar{B}_r^*)/2$, (the star superscript stands for complex conjugate), and a part oscillating at the double of the supply frequency (DSF) $F_{x\,dsf}=-\mathrm{Re}(\bar{j}_\theta\bar{B}_r e^{-2\mathrm{i}\omega t})/2$, which has a phasor (with double bar to indicate DSF time fluctuation): $\bar{\bar{F}}_{x\,dsf}=-\bar{j}_\theta\bar{B}_r/2$. Using the dimensionless solution above, this can be written $F_{x\,avg}=F_{ref}f_{x\,avg}$ and $\bar{\bar{F}}_{x\,dsf}=F_{ref}\bar{\bar{f}}_{x\,dsf}$, with:

$$F_{ref}=\frac{k\mu_0 J_{peak}^2}{2} \;,\; f_{x\,avg}=R_{mB}\Re\left[\left(\mathrm{i}\bar{\alpha}-u\frac{\partial\bar{\alpha}}{\partial\xi}\right)\frac{\partial\alpha^*}{\partial\xi}\right] \;,\; \bar{\bar{f}}_{x\,dsf}=R_{mB}\left(\mathrm{i}\bar{\alpha}-u\frac{\partial\bar{\alpha}}{\partial\xi}\right)\frac{\partial\bar{\alpha}}{\partial\xi} \quad (9)$$

Those expressions can be constructed analytically from (6) or (7) and (8), to get the distribution of electromagnetic forces inside the pump. In the thin channel case, the force density will depend only on $\xi$ and will be equilibrated by the pressure rise along the channel (and by friction forces which are typically one or two orders of magnitude lower). In other cases, the non uniform distribution of the forces across the channel is not compatible with a developed velocity profile ($dU/dx$=0), and it will have the velocity profile evolve towards an equilibrium profile described in [7] for infinite pumps. Since we use a uniform velocity profile, we only present results calculated with thin channel hypothesis.
Integrating the average force density $F_{x\,avg}$ over the channel length will give the pressure rise provided by the pump (neglecting friction), and integrating $F_{x\,dsf}$ will give the DSF fluctuation of this pressure rise. We use a numerical integration over the interval $-p-1<\xi/\pi<p+10$ (out of which the force density is negligible), with a step $\delta\xi=\pi/25$.

**Results**

The model was first applied to a pump with $p$=3 pairs of poles as PEMDYN, for $R_{mB}$=8, typical in that facility. Figure 2 shows a typical traveling wave shape at moderate slip ($1-q$=20%), with the different modes contributing to the real part of $f(\xi)$ (in black). The upstream diffusion of each end effect is hardly visible since it affects a very short length, whereas the downstream convection affects the whole inductor and a large zone after it. The inlet wave (dark red), almost compensating the infinite pump solution (light blue) at inlet, propagates downstream with damping, but since it propagates at a different speed, it can be in phase before outlet. Therefore the module of the wave does not increase monotonically from inlet downwards, as shown in Figure 3 where it is plotted for several values of $q$. For lower $q$, the velocity difference between both waves is larger and the interference effect is stronger.

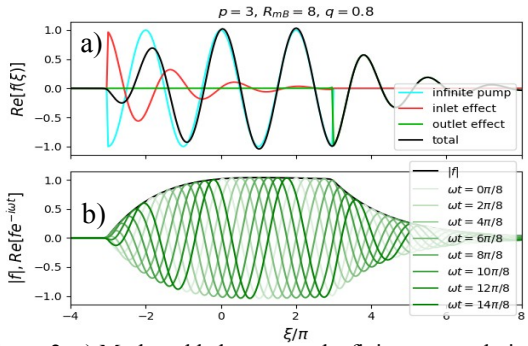


Figure 2: a) Modes added up to get the finite pump solution ; b) resulting traveling wave

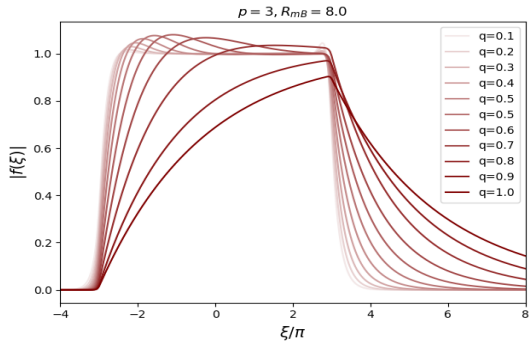


Figure 3: Module of the traveling wave for $p$=3, $R_{mB}$=8 and several values of $q$

Our theory was validated using a numerical axisymmetric model [8] based on the finite volume code Fluent plus a home made induction module. The configuration of Figure 1 b) was modelled with $p$=10, $H_R$=0.005, $H_\lambda$=0.45, $R_{mB}$=8.9 and several values of $q$. The finite volume code calculates the velocity profile, using a uniform profile imposed at inlet ($x$=−6$\lambda$), and a uniform pressure at outlet ($x$=15$\lambda$). Despites its uniform velocity, our theory gives a radial magnetic field close to the numerical calculation (Figure 4), and a theoretical performance curve (Figure 5) corresponding roughly to the electromagnetic term in the numerical code (the total pressure difference is slightly weaker because of friction).

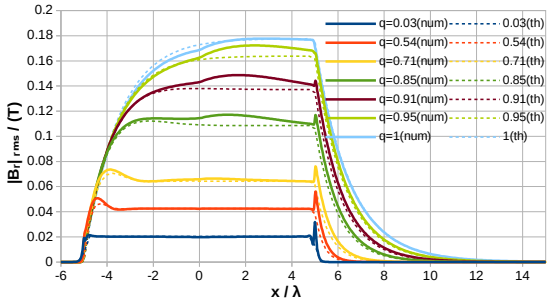


Figure 4: Radial magnetic field: theoretical and numerical

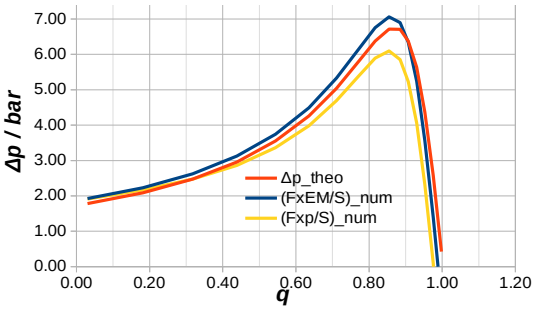


Figure 5: performance curves: theorerical and numerical.

The axial force density distribution is presented in Figure 6 for a typical PEMDYN case ($p$=3, $R_{mB}$=8), and in Figure 7 for an hypothetic pump with 10 poles ($p$=5) and a larger synchronism velocity, wavelength or fluid conductivity ($R_{mB}$=20). This last figure clearly shows the interference effect making the force density oscillate with $\xi$.

As previously described [3], [4], [6], the inlet end effect is responsible for a negative force (directed upstream), on a zone that appears to be longer and longer as the flowrate tends to synchronism. The electromagnetic problem seen from the fluid side is similar to transient diffusion into the channel of a suddenly applied AC field, whereas the fluid is convected downwards: the length of the inlet effect thus increases with $q.R_{mB}$ (and not $R_{mS}$). It appears in our model that a zone with similar length would exist after the inductor end because of the convection of the electromagnetic field after the pump outlet, if the magnetic yokes were long enough. That zone would generate few net pressure but a large amount of DSF fluctuations, and its limitation due to limited yokes will decrease pressure fluctuation but not pressure rise.

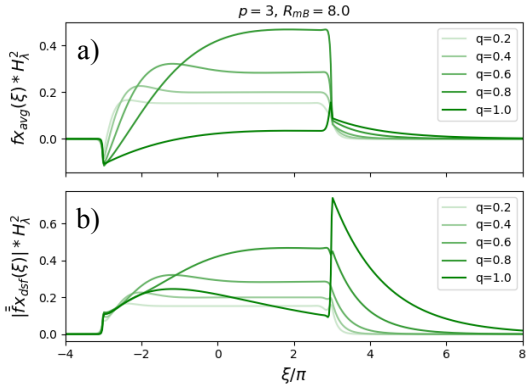


Figure 6: Force density along small pump: a) avg, b) dsf

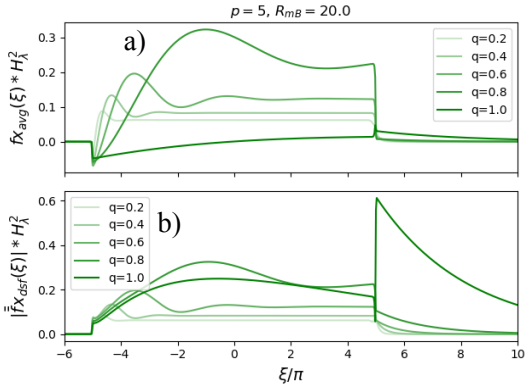


Figure 7: Force density along larger pump: a) avg, b) dsf

Integrating the force distribution, we obtain the pressure difference provided by the pump for any value of $q$ (performance curve at constant current), but also the fluctuation of this pressure difference. Such curves are presented in Figure 8 for $p$=3 and several values of $R_{mB}$. The dimensionless values plotted in that figure should be divided by $H_z^2$, and multiplied by $F_{ref}/k$ to get pressure differences in Pascals. The DSF pressure fluctuation can be 0 even if the module of $\bar{fx}_{dsf}$ is constant along the pump, because its phase evolves along $\xi$. For the infinite pump solution, the phasor is proportional to $e^{2i\xi}$, and integrating from $-p\pi$ to $p\pi$ gives 0. The DSF pressure fluctuation is thus due to end effects.

An infinite pump with thin channel would give a maximum average force density at $R_{mS}$=1, where $H_\lambda^2 fx_{avg}$=0.5 , so that the total dimensionless force would be $H_\lambda^2 fx_{avg}^{tot} = \pi p$ at the maximum point, if we integrate over the finite length without end effects. The maximum of the performance curves such as the ones in Figure 8 a) can be compared to those values, and this work can be repeated for other values of $p$. The results are presented in Figure 9, and shows that the maximum always occur at higher slip than $R_{mS}$=1, especially for a small number of poles where the end effects are more present. Because of the end effects, the maximum pressure provided by the pump is lower than expected from the infinite pump solution, especially if the number of pole pairs is small and expecially for large values of $R_{mB}$.

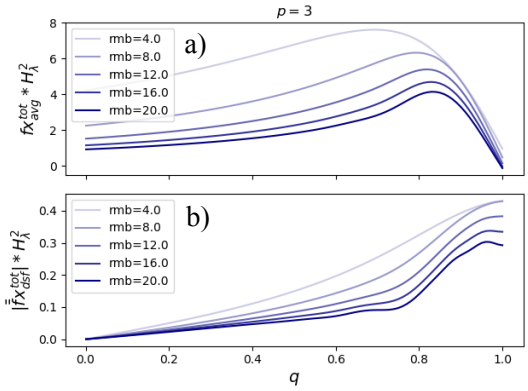


Figure 8: Pressure provided by the pump as a function of flowrate: a) mean value, b) dsf fluctuation

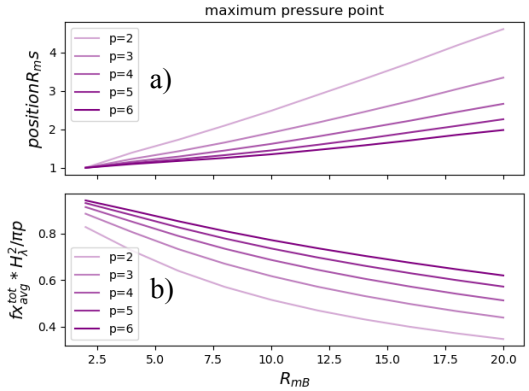


Figure 9: Maximum pressure point of an ALIP with p pairs of poles: a) position, b) value of the maximum

**Conclusion**

This paper presents a simple analytical model to describe the end effects in large size annular linear induction pumps. It gives the real position and value of the maximum pressure point, and thus can be used to rapidely find the limits of the stable working domain of the pump, as well as for parametric studies concerning the pump performance, or pressure fluctuations at $2\omega$.

**References**

[1] A. Gailitis and O. Lielausis, Magnetohydrodynamics 11 (1975) 69-79.
[2] H.Araseki, I.R.Kirillov, G.V.Preslitsky, A.P.Ogorodnikov, Nuclear Engineering and Design 227 (2004) 29-50.
[3] H.R. Kim, Annals of Nuclear Energy 62 (2013), 103-108
[4] M.Pouloujadoff, B.Morel, A.Bolopion, IEEE Transactions on Power Apparatus and Systems 99 (1980), 1172-1180
[5] L.Goldsteins, PhD, Univ. Grenoble Alpes, https://tel.archives-ouvertes.fr/tel-01232570 (2015)
[6] F.Werkoff, Experimental thermal and fluid science 4 (1991) pp 166-170
[7] Y.Delannoy, E.Martin-Lopez, F.Benoit, 18th Int. Symp. on Appl. Electromagn. and Mechanics, Chamonix (2017).
[8] E.Martin-Lopez, Y.Delannoy, F.Benoit, A.Muñoz Medina, R.Martinie, Int.Cong.Adv.Nucl.Pow.Plants, Charlotte, USA (2018)